Application of Image Processing and Circular Statistics to 3D Cellular Alignment

Beth Jelfs and Christopher Gilliam
RMIT University, Melbourne, Australia
E-mail: {beth.jelfs,christopher.gilliam}@rmit.edu.au

Abstract—Alignment and orientation of cells play an important part in the function of biological tissue. Recent developments in bioengineering using 3D scaffolds have created an increased need for computational techniques to measure orientation which extend beyond 2D measures to produce 3D measures of orientation. Initial studies of 3D alignment have focused on determining individual orientations, however, to truly understand the impact these structures have on the cellular alignment we need to understand the overall distribution of the orientations and their statistics. Hence, in this paper we develop an approach for determining 3D cellular alignment based on image gradients and directional statistics. The intensity gradients of the volumetric image are used to construct a 3D vector field and the local dominant orientations of this vector field then determined.

I. INTRODUCTION

Structure at a cellular level is an important aspect in the function of biological tissue. The alignment and orientation of cells and fibres have marked effects on the properties of tissue. For instance, the structural organization of the cell cytoskeleton can impact on functional differentiation of stem cells [1]; orientation of stress fibres can affect cell remodelling [2]; and orientation of actin filaments are important in determining cellular shape and also cell movement [3].

However, 2D alignment of 3D structures do not necessarily give the full picture, with 3D structures of tissue often critical to the function of the tissue. At the same time, cells which have been cultured on a 2D substrate vs those which have been embedded in a 3D media have been shown to produce different orientations [4]. Accordingly, recent developments in tissue engineering have been designed to control the growth of cells and thus the cellular alignment using 3D scaffolds. By engineering scaffolds for use in biomanufacturing, the patterns of the scaffold can be used to guide cell alignment [5]. Similarly encapsulating the cells in hydrogels can result in engineered tissues with complex structures [6]. Hence, being able to quantify cellular alignment within 3D cell populations is necessary for understanding tissue architecture or engineering tissue with the desired structures and validating the outcomes.

Using imaging to understand the 3D cellular structure both for individual cells and for the construction/reconstruction of tissue has been of interest for a number of years [7]. However, with increased access to large amounts of 3D imaging data at a cellular level, analysis of 3D data is gaining larger traction and a number of different computational approaches to 3D assessment of cellular structure have been proposed [8], [9]. In particular the use of structure tensors has been shown to be an effective method for determining fibre orientation in 3D [10], [11].

While the use of structure tensors may be effective when calculated globally across a volume, in many cases we need to estimate orientations on a local level to account for differences in orientation of different objects. In this case over a small local window the performance of the structure tensor is similar to that of the image intensity gradients on which it is based. Using image intensity gradients directly also circumvents the need to calculate the large number of eigenvalue decompositions required to estimate the orientation from the structure tensors, vastly reducing the computation time. In [10] the authors present a toolbox for the assessment of the morphology of fibres in bioengineered scaffolds based on the use of structure tensors. In this case, to overcome the need to assess the eigenvalues associated with each of the structure tensors for every voxel, the original data is preprocessed to give a binary skeleton and only the orientation of these points are used.

However, one of the aspects which is not addressed in [10] is whether the resultant local orientations are actually meaningful. For this, analysis of the spherical distribution based on the eigenvalues of each of the structure tensors is required. At the same time not only do we want to know whether individual estimates of orientation are meaningful we also want to understand the overall distribution of the orientations across the entire volume. In [11] structure tensors are also used to estimate the orientation; following which an overall orientation of the volume is estimated and spherical statistics are employed to determine the dispersion of the distribution of orientations. This approach provides statistical information about the volume but the estimation of the global principal orientation assumes a structure on the local orientations which may not be valid.

One approach to ensuring the validity of the local orientation estimates is to determine whether the distribution of the local region is non-spherical. To be spherical requires the data to be circular in all three coordinate planes. Hence, it is possible to use 2D measures of circularity of the data to determine the sphericity of the local region. In terms of second order statistcs, one computationally efficient measure of circularity (propriety), is the degree of impropriety based on the circularity coefficients [12], [13]. By using the image intensity gradients to determine the degree of impropriety in each of the 3 coordinate planes, only those voxels whose local
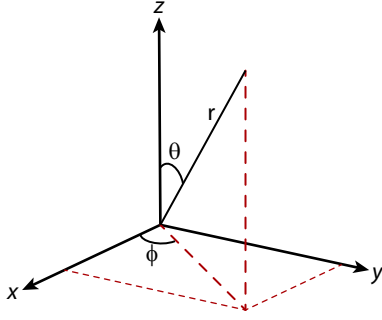
Fig. 1. Diagram illustrating the relationship between spherical polar coordinates, (r, θ, ϕ), and Cartesian coordinates, (x, y, z). Note that θ represents the elevation angle and ϕ the azimuth angle.

region are considered significantly improper in at least one plane are included in the orientation estimation.

In this paper we propose a method to estimate orientations from 3D data which determines the statistical validity of the local orientation estimates and the spherical statistics of the entire volume. We propose using the image intensity gradients directly to estimate orientation. The degree of impropriety of the gradients is then used to estimate the sphericity of the local regions of each voxel and only those voxels which are considered non-spherical are included in the orientation estimation. For the orientation estimation we use a maximum-likelihood estimator [14] to determine the dominant orientation of the selected voxels following which the distributions of the orientations across the entire volume are assessed. The proposed approach is tested on simulations with volumes containing fibres with varying alignments and fibrous composite scaffolds [10] with the results showing the proposed method is capable of distinguishing different structures.

II. ESTIMATION OF LOCAL 3D ORIENTATION

In this section we outline our approach to estimating the local dominant orientation of a 3D object in volumetric images. Instead of assuming a certain type of 3D structure, e.g. cylindrical fibres of certain diameter, or segmenting the data, our approach is based on the relationship between the local 3D orientation and the vector field formed from the gradients of the image intensity. This relationship and our approach are outlined as follows.

In terms of notation, the local orientation is defined using the spherical coordinate system (r, θ, ϕ), where r represents the radius, θ is the elevation angle and ϕ is the azimuth angle. The elevation angle is measured relative to the positive z-axis and the azimuth angle is measured relative to the positive x-axis, in the (x, y)-plane. An illustration of these coordinates are shown in Fig. 1. Finally, for reference, the mapping between the standard Cartesian coordinate system and the spherical system is:

$$\begin{bmatrix} x \\ y \\ z \end{bmatrix} = \begin{bmatrix} r \sin\theta\cos\phi \\ r \sin\theta\sin\phi \\ r\cos\theta \end{bmatrix} \longleftrightarrow \begin{bmatrix} r \\ \theta \\ \phi \end{bmatrix} = \begin{bmatrix} \sqrt{x^2 + y^2 + z^2} \\ \cos^{-1}\left(\frac{z}{r}\right) \\ \tan^{-1}\left(\frac{y}{x}\right) \end{bmatrix} \quad (1)$$

To cover the whole sphere requires $\theta \in [0, \pi]$ and $\phi \in [0, 2\pi]$. However, 3D orientations are a form of axial data [15], [16], accordingly, the orientation at (θ, ϕ) is equivalent to the orientation at $(\pi - \theta, \phi + \pi)$. As a consequence, we consider only half of the sphere and restrict the azimuth angle to $\phi \in [0, \pi]$.

A. Image Intensity Gradient Vs Local Orientation

Our approach relies upon the computation of the image intensity gradient $\vec{G}(x, y, z)$ from the volumetric image $I(x, y, z)$. This gradient is a vector field that is constructed from the differentials of $I(x, y, z)$ in the x, y and z directions, i.e.:

$$\vec{G}(x, y, z) = \begin{bmatrix} G_x(x, y, z) \\ G_y(x, y, z) \\ G_z(x, y, z) \end{bmatrix}, \quad (2)$$

where G_i represent the differential of I with respect to the ith direction. In practice, to account for noise in the image, the differential operator is combined with a Gaussian filter [11], [17], [18]. Accordingly, the ith components of $\vec{G}$, where $i \in \{x, y, z\}$, is obtained via the following convolution

$$G_i(x, y, z) = h_i(x, y, z) * I(x, y, z), \quad (3)$$

where $*$ is the convolution operator and $h_i(x, y, z)$ is the derivative of a Gaussian window with respect to i:

$$h_i(x, y, z) = \frac{2i}{\sigma^2} \exp\left\{ -\frac{x^2 + y^2 + z^2}{\sigma^2} \right\}.$$

In terms of implementation, we limit this derivative filter to a compact support defined by a $(2s + 1) \times (2s + 1) \times (2s + 1)$ cube, i.e. the filter is non-zero for the voxels $x, y, z \in [-s, s]$, and we set $\sigma = (s + 2)/4$.

The importance of this vector field $\vec{G}$ is that it encodes the structural information present in the image. The magnitude of $\vec{G}$ is large at the boundary of objects – a property used in edge detection – and the corresponding direction at these object boundaries is normal to the orientation of the boundary. In other words, the direction of the gradient vectors at an object boundary are normal to the local dominant orientation that we wish to estimate. An illustration of this relationship is shown in Fig. 2(a). Accordingly, to determine the local dominant orientation, we need to estimate the vectors normal to $\vec{G}$ and extract their orientation. In 2D this problem is straightforward, the normal vectors are at 90° to the gradient vectors [18]. In 3D however the relationship is more complicated as a normal vector is defined relative to a plane rather than a single vector. Thus, we employ tools from spherical statistics to determine the local dominant orientation from $\vec{G}$. In particular, we model $\vec{G}$ locally using a girdle distribution as discussed in the next section.

B. Girdle Distributions

In spherical statistics, a girdle distribution is used to model a set of data points defined in spherical polar coordinates (θ, ϕ) that are concentrated on a great circle [15], [16], i.e. the data points all reside in the same plane. The distribution is

(a) Gradient vectors vs local dominant orientation
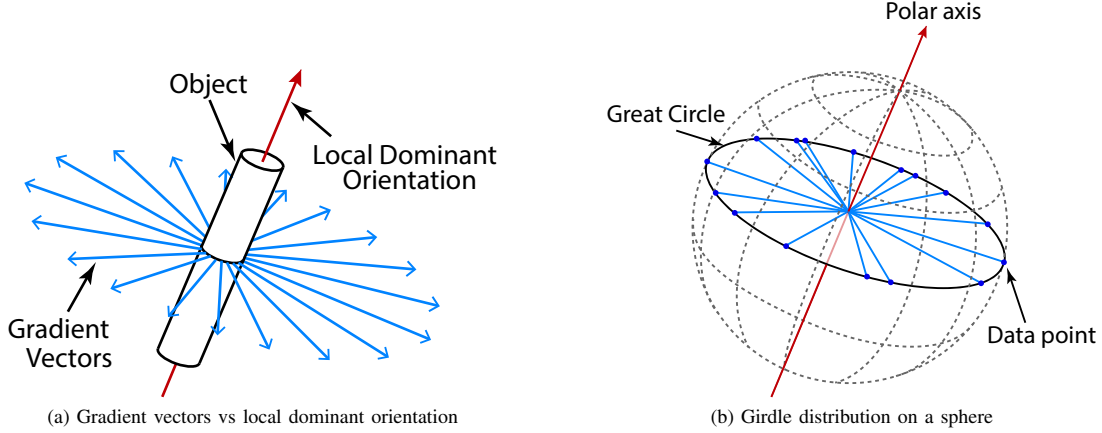
(b) Girdle distribution on a sphere

Fig. 2. Diagrams illustrating the relationship between the local dominant orientation and a girdle distribution on a sphere. Part (a) shows a set of image intensity gradient vectors estimated from an object at a certain orientation. The gradient vectors reside in a plane that is normal to the local dominant orientation. Part (b) shows a set of data points drawn from a girdle distribution with a certain polar axis. Similar to the local dominant orientation, the polar axis is normal to the great circle where the data points reside.

characterised by a concentration parameter γ, which describes the concentration of the points around the circle, and the polar axis, which is the normal vector to the great circle. An illustration of a girdle distribution is shown in Fig. 2(b). Importantly, the figure highlights the similarity between a girdle distribution and the local dominant orientation. The image intensity gradients at the boundary of an object all reside in the same plane. Which if we compare Fig. 2(a) and Fig. 2(b) we can see this is conceptually the same as the data drawn from a girdle distribution. Therefore, if these planes coincide then the polar axis is aligned with the local dominant orientation. Thus, the problem of determining the local dominant orientation can be posed as determining the polar axis of a girdle distribution assuming the image intensity gradients are data points drawn from the distribution [15].

This link between the girdle distribution and the local 3D orientation of an object is leveraged in methods based on the structure tensor. If the image intensity gradients used to construct the structure tensor follow a girdle distribution then the polar axis is equivalent to the eigenvector corresponding to the smallest eigenvalue of the tensor [15]. Although the structure tensor is only a 3×3 matrix, performing local eigenvalue decompositions to gain a per voxel estimate of the orientation is time consuming for a 3D volume [11], [10]. Accordingly, in this paper we consider an alternative approach to the orientation estimation problem based on the work of Selby [14]. Selby proposed the following probability density function for a girdle distribution

$$
\begin{aligned}
g(\theta, \phi; \gamma, \alpha, \beta) = &\frac{\gamma \sin(\theta)}{4\pi \left(1 - e^{-\gamma}\right)} \cdot \\
&\exp\left(-\gamma \left|\cos\alpha\cos\theta + \sin\alpha\sin\theta\cos(\phi - \beta)\right|\right)
\end{aligned}
\tag{4}
$$

where (θ, ϕ) is the spherical coordinate describing the direction of the vector, γ is the concentration parameter and (α, β) is the polar axis of the distribution. Based on this density

function, Selby derived the following maximum-likelihood estimate for the polar axis given N data points drawn from the distribution:

$$
(\hat{\alpha}, \hat{\beta}) = \arg\min_{\alpha, \beta} \left\{ Z(\alpha, \beta) \right\}
\tag{5}
$$

where Z is the likelihood function

$$
Z(\alpha, \beta) = \sum_{n=1}^{N} \left| \cos\alpha\cos\theta_n + \sin\alpha\sin\theta_n \cos\left(\phi_n - \beta\right) \right|,
$$

and (θ_n, ϕ_n) are the elevation-azimuth angles of the ith data point. In the next section we use this maximum-likelihood estimator as the basis for our orientation algorithm.

C. Proposed Algorithm

Our proposed algorithm comprises four steps as follows. The first step of our algorithm is to compute the image intensity gradient $\vec{G}$ using the convolution operation defined in (3). For this paper, we set $s = 6$ in the derivative filter h_i. As a consequence the support of the filter is $11 \times 11 \times 11$ voxels.

The second step is to classify the vectors in the image gradient into two groups: spherical and non-spherical. This classification is achieved by testing the sphericity of the gradient vectors within a local region and then repeating the test for every vector in $\vec{G}$. The details of this local sphericity test are covered in Section III. For reference, we set the local region to be $7 \times 7 \times 7$ voxels.

The next step is to determine the local dominant orientation for the vectors classified as non-spherical. To estimate this orientation, we adapt Selby's [14] maximum-likelihood estimator for determining the polar axis of a girdle distribution. Specifically, for each non-spherical vector, we estimate the polar axis angles given a local region $\mathcal{W}$ centred around the vector. Note that α and β equate respectively to the elevation

and azimuth angles of the local orientation. The estimate is obtained by solving the following minimisation:

$$\arg\min_{\alpha,\beta} \sum_{\mathbf{x}\in\mathcal{W}} G(\mathbf{x})\left|\cos(\alpha)\cos\left(\hat{\theta}(\mathbf{x})\right)\right.$$
$$\left.+ \sin(\alpha)\sin\left(\hat{\theta}(\mathbf{x})\right)\cos\left(\hat{\phi}(\mathbf{x})-\beta\right)\right| \quad (6)$$

where $\mathbf{x}=(x,y,z)^{\mathsf{T}}$ denotes the voxel coordinates, $G(\mathbf{x}) = |\vec{G}(\mathbf{x})|$ is the magnitude of the image intensity gradient, and $\hat{\theta}(\mathbf{x})$ and $\hat{\phi}(\mathbf{x})$ are respectively the estimates of elevation and azimuth angle. These estimates are determined by applying the transformation in (1) to the image gradient, i.e.

$$\hat{\theta}(\mathbf{x}) = \cos^{-1}\left(\frac{G_z(\mathbf{x})}{G(\mathbf{x})}\right), \quad\text{and}\quad \hat{\phi}(\mathbf{x}) = \tan^{-1}\left(\frac{G_y(\mathbf{x})}{G_x(\mathbf{x})}\right).$$

Note that we have adapted Selby's original formulation of the maximum-likelihood estimate to include the magnitude of the image vector as a weight coefficient. The local region $\mathcal{W}$ is set to $11\times11\times11$ voxels.

In terms of implementation, we use an iterative method to solve the minimisation in (6) – a closed-form expression does not exist. Our iterative method involves calculating the argument of the minimisation for a uniform grid of α and β values and choosing the pair which coincide with the minimum value. Although the accuracy of such a solution is limited to the grid size, it has two benefits: first, for a given (α,β)-pair the argument of the minimisation can be computed efficiently using blockwise multiplication for every non-spherical vector. Second, by using this parallel computation, the search space of the algorithm is reduced to the size of the grid, i.e. the algorithm can be sped up by reducing the number of (α,β)-pairs in the grid. For this paper, we consider a 2D grid that spans $\alpha,\beta\in[0,180°]$ in steps of $1°$ for each angle.

The final step in the algorithm is to assess the distribution of the estimated local orientations over the whole volume. To perform this assessment, the set of local orientation angles, $\{\hat{\alpha}_n,\hat{\beta}_n\}_{n=1}^N$, are converted to a set of unit vectors, $\{\vec{v}_n\}_{n=1}^N$, where N is the number of data points. Note that, as the orientations are axial data, the azimuth angle $\hat{\beta}$ is multiplied by 2 so that the vectors can cover the whole unit sphere. Given these unit vectors, the assessment of their distribution comprises four measures: the first three are the non-circularity measures detailed in Section III. The final measure is the mean resultant length from spherical statistics, which is calculated as [15], [16]:

$$\bar{R} = \left|\frac{1}{N}\sum_n \vec{v}_n\right|. \quad (7)$$

This quantity varies between 0 and 1; $\bar{R}\approx0$ indicates the vectors are widely dispersed whereas $\bar{R}\approx1$ indicates the vectors are heavily concentrated [16]. The non-circularity measures are used to quantify the sphericity of the overall distribution and the mean resultant length quantifies the concentration of the vectors.

III. TESTING DISTRIBUTION OF ORIENTATION

Determining the sphericity of data is not a straightforward problem, tests are either tailored to certain distributions or computationally intensive which preclude their use when requiring large numbers of tests on local regions with unknown distributions. However, for data to be spherically distributed requires that the data is also circularly distributed when projected into each of the 3 coordinate planes (x,y), (x,z) and (y,z). By taking advantage of this knowledge we can employ measures of circularity which are generally more tractable.

Whether determining the sphericity or circularity of data it is worth considering that the orientation of the data is only one aspect and to fully describe a vector we also require a magnitude. Typically, both spherical and circular distributions sit on the unit sphere/circle, and while this can be useful if we are considering only the angular distribution of the data this gives no indication of the magnitude of the vectors. An alternative is to form complex data from the vectors such that a vector in the (x,y)-plane, $\vec{v}(x,y)$, can be represented as the complex number $x+\jmath y$, and similarly for the other two planes. From which we can use complex statistics to assess the circularity of the data allowing us to take advantage of the entire information contained with in the vector not just the orientation.

For a complex variable to be circular requires the probability distribution to be invariant under rotation in the complex plane. A weaker, more tractable, property however can be constructed in terms of only the second order statistics; if the variable is uncorrelated with its complex conjugate then it is considered second order circular or *proper*. Meaning that for the complex variable $\mathbf{w}\in\mathbb{C}^N$ constructed from the two real variables $\mathbf{w}_r\in\mathbb{R}^N$ and $\mathbf{w}_i\in\mathbb{R}^N$ such that $\mathbf{w}=\mathbf{w}_r+\jmath\mathbf{w}_i$, the covariance matrix is $\mathbf{C}=E\{\mathbf{w}\mathbf{w}^H\}$ and the complimentary covariance is $\widetilde{\mathbf{C}}=E\{\mathbf{w}\mathbf{w}^T\}$. A proper complex variable has $\widetilde{\mathbf{C}}=0$, otherwise the variable is improper, with impropriety implying non-circularity [13].

Using the second order statistics of the data, a test for impropriety can be constructed based on the circularity coefficients of the data. Starting with the coherence matrix

$$\mathbf{M} = \mathbf{C}^{-1/2}\widetilde{\mathbf{C}}\mathbf{C}^{-T/2}, \quad (8)$$

we can define the Takagi's factorization (a special singular value decomposition) which gives

$$\mathbf{M} = \mathbf{F}\mathbf{K}\mathbf{F}^T \quad (9)$$

where $\mathbf{F}$ is a complex unitary matrix and $\mathbf{K} = \mathrm{diag}(k_1,k_2,\ldots,k_N)$ where $\{k_n\}_{n=1}^N$ are the canonical correlations also known as the circularity coefficients [12], [13]. These circularity coefficients can be used to measure the degree of impropriety of the data based on [12]

$$\ell = 1 - \prod_{n=1}^N\left(1-k_n^2\right) = 1 - \frac{\det\mathbf{C}}{\det^2\mathbf{C}} \quad (10)$$

where

$$\underline{\mathbf{C}} = \begin{bmatrix} \mathbf{C} & \widetilde{\mathbf{C}} \\ \widetilde{\mathbf{C}}^* & \mathbf{C}^* \end{bmatrix}$$

and $\ell = 0$ equates to proper data and $\ell = 1$ to proper. For a scalar variable w with covariance $C = E\{|w|^2\}$ and complementary covariance $\widetilde{C} = E\{w^2\}$ the degree of impropriety becomes

$$\ell = \frac{|\widetilde{C}|^2}{C^2}. \tag{11}$$

Using (11) we can test the impropriety or non-circularity of each of the local regions in all 3 coordinate planes. Due to only requiring calculation of the complex second order statistics this method is computationally efficient. Meaning that despite needing to calculate in all three planes when dealing with a large number of local regions this is still a more efficient method than calculating a single spherical measure.

IV. RESULTS

In this section we present the results of our proposed algorithm on both synthetic and real data. The code to reproduce these results can be downloaded from the following repository https://github.com/beteje/Orientation.

A. Data Generation

To test our algorithm, we generated synthetic volumes that mimic fibrous data and varied the alignment of the fibres within the volumes. We generated these volumes based on the method outlined in [10]. In brief, a volume is $256 \times 256 \times 256$ voxels in size and comprise 100 simulated fibres. Each fibre is parameterised in terms of their radius, length, position and orientation. The radius of the fibres vary between 2 and 10 voxels, and their lengths vary between 0.3 and 0.9 of the volume size. The position of the fibres is random within volume provided none of the fibres overlap with another. The orientation of the fibres is controlled directly to set the overall organisation of the fibres.

Using this method, we generate four volumes with the following types of fibre organisation:
1) **Random**: The fibres are randomly orientated. The elevation and azimuth angles for the fibres are randomly drawn from the range $0° - 180°$.
2) **Range**: The fibres are more organised and their orientation is concentrated to a certain range. Their elevation angles vary between $70° - 100°$ and their azimuth angles between $90° - 120°$.
3) **Double**: There are two distinct orientations of the fibres. For one set of fibres, their elevation angles vary between $30° - 35°$ and their azimuth angles vary between $70° - 75°$. For the other set, their elevation angles vary between $110° - 115°$ and their azimuth angles between $150° - 155°$.
4) **Single**: All of the fibres are orientated in one direction. Their elevation angles vary between $30° - 35°$ and their azimuth angles vary between $70° - 75°$.

TABLE I
MEASURES OF NON-CIRCULARITY AND SPHERICAL MEAN RESULTANT LENGTH FOR DIFFERENT DATASETS.

	PSNR	ℓ_{XY}	ℓ_{YZ}	ℓ_{XZ}	$\bar{R}$
	30 dB	0.83	0.94	0.94	0.96
Single	20 dB	0.88	0.95	0.96	0.98
	10 dB	0.85	0.95	0.94	0.97
	30 dB	0.80	0.80	0.50	0.35
Double	20 dB	0.81	0.82	0.53	0.39
	10 dB	0.77	0.86	0.62	0.57
	30 dB	0.64	0.80	0.51	0.89
Range	20 dB	0.65	0.82	0.55	0.91
	10 dB	0.67	0.83	0.51	0.91
	30 dB	0.01	0.18	0.19	0.03
Random	20 dB	0.02	0.20	0.24	0.05
	10 dB	0.05	0.30	0.41	0.07
Random Scaffold Data	-	0.31	0.34	0.72	0.36
Aligned Scaffold Data	-	0.73	0.57	0.07	0.89

We also test the performance of our algorithm under varying amounts of noise. Specifically, for each of the volumes described above, we add white Gaussian noise to the images to obtain PSNR values of 30dB, 20dB and 10dB.

B. Synthetic Simulations

For the first set of simulations we visualised the orientation estimates obtained from the data containing the concentrated range of angles and the completely random data, both for a PSNR of 30dB. Figure 3 shows the results obtained for the range data. Firstly, we note that when comparing the simulated fibres in Fig. 3(a) and the estimated fibres in Fig. 3(c) we can see that the use of the non-circularity measures successfully distinguishes the fibres from the background noise. However, due to the effects of derivative filters in the estimation of the gradient vectors the fibres dilate, meaning the estimated fibres have a slightly larger radius than the true radius.

To aid the visualisation of the orientation angles each combination of azimuth and elevation angles are given a unique colour, as illustrated in Fig. 3(b). As can be seen from the shades of the fibres in both Fig. 3(a) and Fig. 3(c), the angles of the estimations are similar to those of the original fibres. This is supported by the histograms of the estimated angles where the majority of angle estimates fall between the $90° - 120°$ range for the azimuth and $70° - 100°$ degree range for the elevation.

Figure 4 shows visualisation of the results obtained from the random data. Again we can see that the estimated fibres and angles in Fig. 4(c) correspond to those of the actual fibres in Fig. 4(a). In this case we can see there are few fibres which have a mottled effect, this primarily down to imperfections in the visualisation. Fibres which are vertical can have an angle which is close to $0°$ or close to $180°$. As the visualisation uses increasing saturation to indicate increasing elevation any slight changes around the $0°$ and $180°$ angles will lead to a
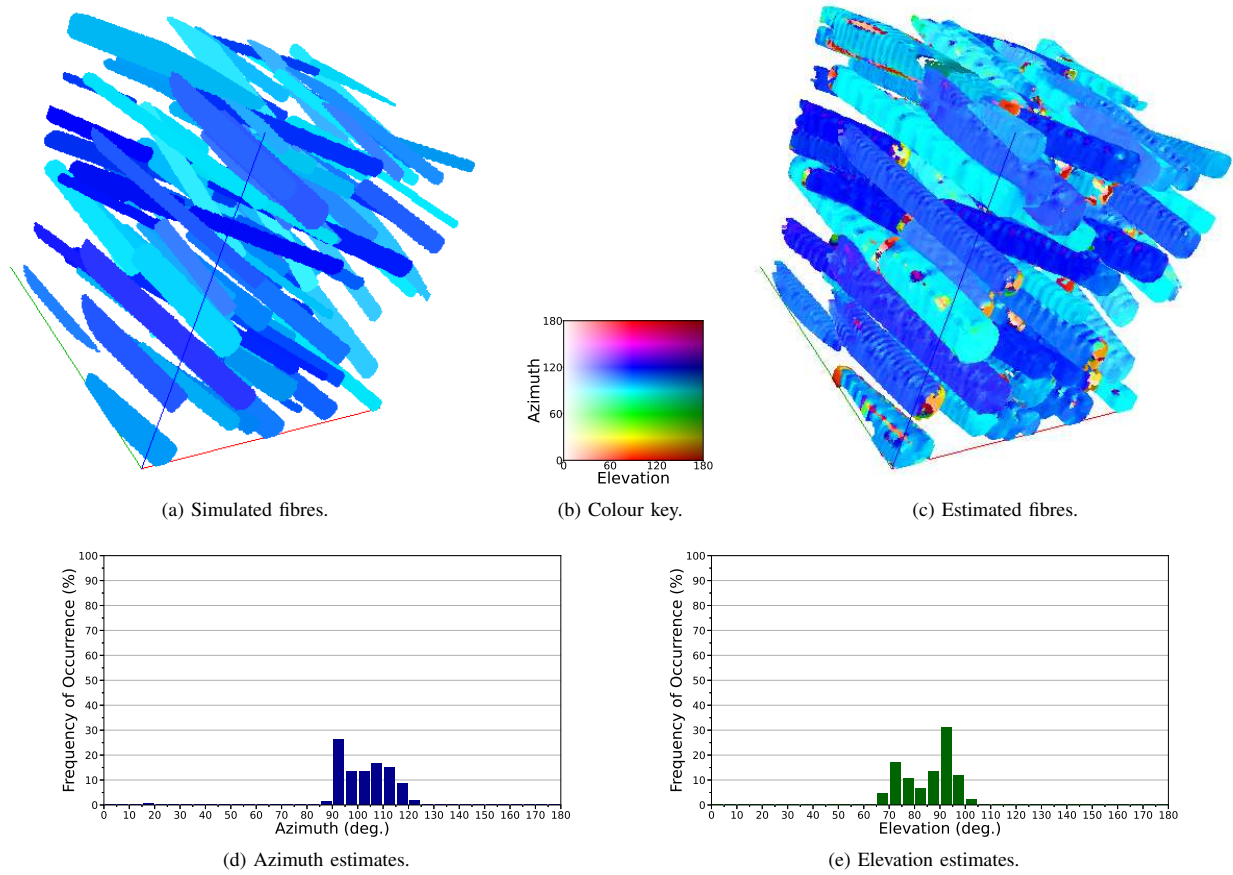
(a) Simulated fibres.

(b) Colour key.

(c) Estimated fibres.

(d) Azimuth estimates.

(e) Elevation estimates.

Fig. 3. Results for fibrous data with a range of angles - azimuth angles $90° - 120°$ and elevation angles $70° - 100°$ with PSNR = 30dB. (a) The true locations and angles of the simulated fibres. (b) The colour key for elevation and azimuth combinations. (c) The estimated fibres. (d) The distribution of the estimated azimuth angles. (e) The distribution of the estimated elevation angles.

combination of very light and very dark shades of the same colour.

Having established that the proposed method could accurately estimate data with different alignments, we next investigated the robustness of the method to noise. Figure 5 shows the histograms of the distributions of the estimated angles for the single data for different noise levels and Fig. 6 shows the histograms for the double data. Both figures indicate that the proposed method could accurately determine the angles of the fibres. However, as the amount of noise increased there was an increase in the spread of the angle estimates around the true angles. If we consider the double data in Fig. 6, particularly the elevation data, we can see that as the noise increases the distribution of the estimates changes which can be accounted for by more of the voxels being considered noise rather than fibres.

Finally, to quantify the estimation results, Table I lists results of the non-circularity tests for each of the coordinate planes, ℓ_{XY}, ℓ_{XZ} and ℓ_{YZ} and the spherical mean resultant length $\bar{R}$. If we compare the single data with the random data

we can see the single data has high non-circularity across all planes and also high resultant lengths for all noise levels, conversely the random data has very low non-circularity results and also low resultant lengths. These results support the visual results indicating that the single data has high non-circularity and also the alignment has a very concentrated direction whereas the random data has low non-circularity and very dispersed orientations. Looking at the results for the range data we can see moderate levels of non-circularity but the high mean resultant lengths indicate that the data is still directional. Whereas the double data has high non-circularity but with lower mean resultant length indicating that the data is non-circular but with less concentrated direction.

C. Real Data

Having tested the proposed method on simulated data we next tested the data on fibrous scaffold data from [10], this data consisted of two different datasets one with aligned structures and one with random structures. Visualisations of the obtained estimates are presented in Fig. 7 and the corresponding non-circularity and mean resultant length values are given in
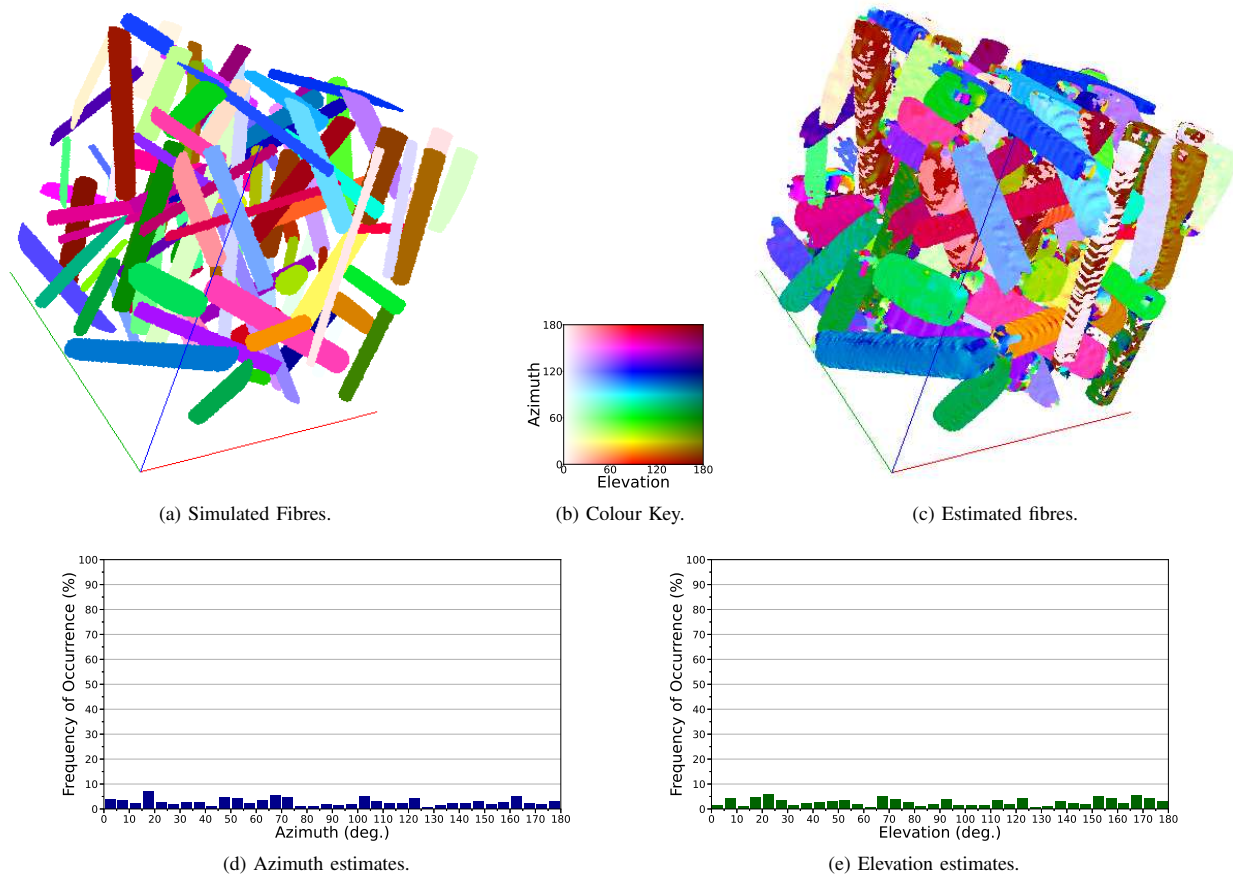
(a) Simulated Fibres.   (b) Colour Key.   (c) Estimated fibres.

(d) Azimuth estimates.   (e) Elevation estimates.

Fig. 4. Results for fibrous data with random - azimuth angles $0° - 180°$ and elevation angles $0° - 180°$ with PSNR = 30dB. (a) The true locations and angles of the simulated fibres. (b) The colour key for elevation and azimuth combinations. (c) The estimated fibres. (d) The distribution of the estimated azimuth angles. (e) The distribution of the estimated elevation angles.

Table I. From the visualisations of the data it is clear that that there is more order to the aligned data. However, the results in Table I indicate that the random data has moderately high non-circularity in the (y, z)-plane, which is supported by the histograms of the angle estimates in Fig. 7(d) and Fig. 7(f) which whilst dispersed across all angles do indicate a slight preferential direction. However the low value of the mean resultant length indicates that this data is not well organised. For the aligned data there are more distinct peaks in the histograms shown in Fig. 7(e) and Fig. 7(g) which are supported by the higher value of the mean resultant length.

V. CONCLUSIONS

In this paper we have proposed a method for estimating and assessing local orientation in 3D data. Our method is based on constructing image intensity gradients, testing their sphericity at a local level, estimating local 3D orientation in regions where the gradients are non-spherical and assessing the distribution of these estimates. To test local sphericity per voxel, we use concepts found in complex statistics, namely the degree of impropriety or non-circularity. By computing the

local non-circularity per voxel we are able to classify spherical and non-spherical regions of the image gradient. Using this classification, our method estimates the local orientation at the non-spherical voxels using a maximum-likelihood estimator. Once these estimates have been obtained, we assess their distribution globally again using the degree of non-circularity and also the spherical mean-resultant length of the data. Key to our proposed method is that each of the steps can be efficiently implemented. We have demonstrated the efficacy of our method on both synthetic and real data.

REFERENCES

[1] M. D. Treiser, E. H. Yang, S. Gordonov, D. M. Cohen, I. P. Androulakis, J. Kohn, C. S. Chen, and P. V. Moghe, "Cytoskeleton-based forecasting of stem cell lineage fates," *Proceedings of the National Academy of Sciences*, vol. 107, no. 2, pp. 610–615, 2009.
[2] S. Pellegrin and H. Mellor, "Actin stress fibres," *Journal of Cell Science*, vol. 120, no. 20, pp. 3491–3499, 2007.
[3] J. Borejdo and S. Burlacu, "Measuring orientation of actin filaments within a cell: orientation of actin in intestinal microvilli," *Biophysical Journal*, vol. 65, no. 1, pp. 300–309, 1993.
[4] K. Chen, A. Vigliotti, M. Bacca, R. M. McMeeking, V. S. Deshpande, and J. W. Holmes, "Role of boundary conditions in determining cell
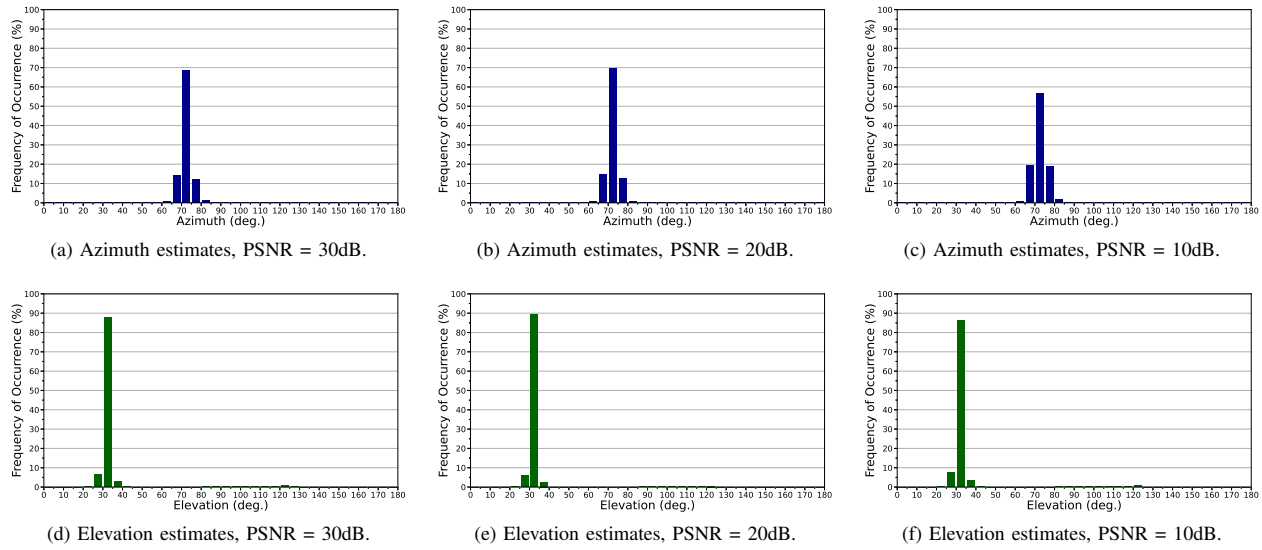
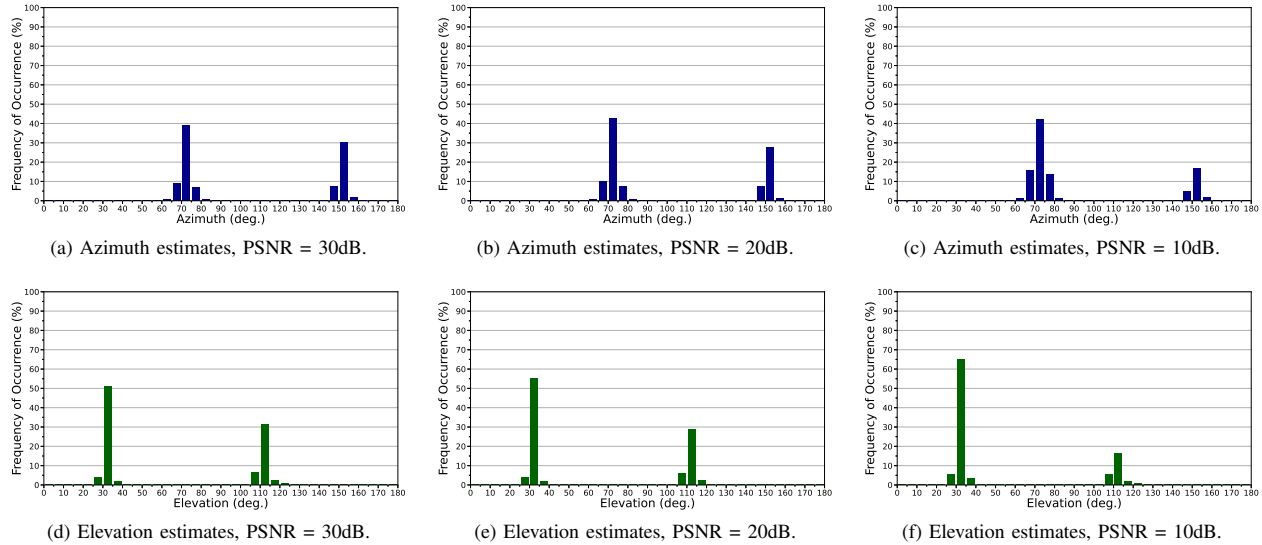Fig. 5. Histograms of the distributions of estimated angles for the single angle data - azimuth angles $70° - 75°$ and elevation angles $30° - 35°$.

Fig. 6. Histograms of the distributions of estimated angles for the double angle data - azimuth angles $70° - 75°$ & $150° - 155°$ and elevation angles $30° - 35°$ & $110° - 115°$.

alignment in response to stretch," *Proceedings of the National Academy of Sciences*, vol. 115, no. 5, pp. 986–991, 2018.

[5] W. Zhang, Z. Wang, C. Xie, X. Wang, F. Luo, M. Hong, R. Zhou, C. Ma, N. Lin, J. Zhang, X. Hu, J. K. Y. Chan, F. Wen, and Y. Wang, "Scaffold with micro/macro-architecture for myocardial alignment engineering into complex 3D cell patterns," *Advanced Healthcare Materials*, vol. 8, no. 22, p. 1901015, 2019.

[6] H. Aubin, J. W. Nichol, C. B. Hutson, H. Bae, A. L. Sieminski, D. M. Cropek, P. Akhyari, and A. Khademhosseini, "Directed 3D cell alignment and elongation in microengineered hydrogels," *Biomaterials*, vol. 31, no. 27, pp. 6941–6951, 2010.

[7] D. J. Fishkind and Y. L. Wang, "Orientation and three-dimensional organization of actin filaments in dividing cultured cells." *The Journal of Cell Biology*, vol. 123, no. 4, pp. 837–848, 1993.

[8] C. Castilla, M. Maska, D. V. Sorokin, E. Meijering, and C. O. de Solorzano, "3-d quantification of filopodia in motile cancer cells,"

IEEE Transactions on Medical Imaging, vol. 38, no. 3, pp. 862–872, 2019.

[9] K. R. Carney, C. D. Bryan, H. B. Gordon, and K. M. Kwan, "LongAxis: A MATLAB-based program for 3D quantitative analysis of epithelial cell shape and orientation," *Developmental Biology*, vol. 458, no. 1, pp. 1 –11, 2020.

[10] R. Shkarin, A. Shkarin, S. Shkarina, A. Cecilia, R. A. Surmenev, M. A. Surmeneva, V. Weinhardt, T. Baumbach, and R. Mikut, "Quanfima: An open source Python package for automated fiber analysis of biomaterials," *PLOS ONE*, vol. 14, no. 4, pp. 1–20, 04 2019.

[11] W. J. Kowalski, F. Yuan, T. Nakane, H. Masumoto, M. Dwenger, F. Ye, J. P. Tinney, and B. B. Keller, "Quantification of cardiomyocyte alignment from three-dimensional (3D) confocal microscopy of engineered tissue," *Microscopy and Microanalysis*, vol. 23, no. 4, pp. 826–842, 2017.

[12] P. J. Schreier, "The degree of impropriety (noncircularity) of complex

(a) Estimates of random structures.

(b) Colour key.

(c) Estimates of aligned structures.

(d) Azimuth estimates, random.

(e) Azimuth estimates, aligned.

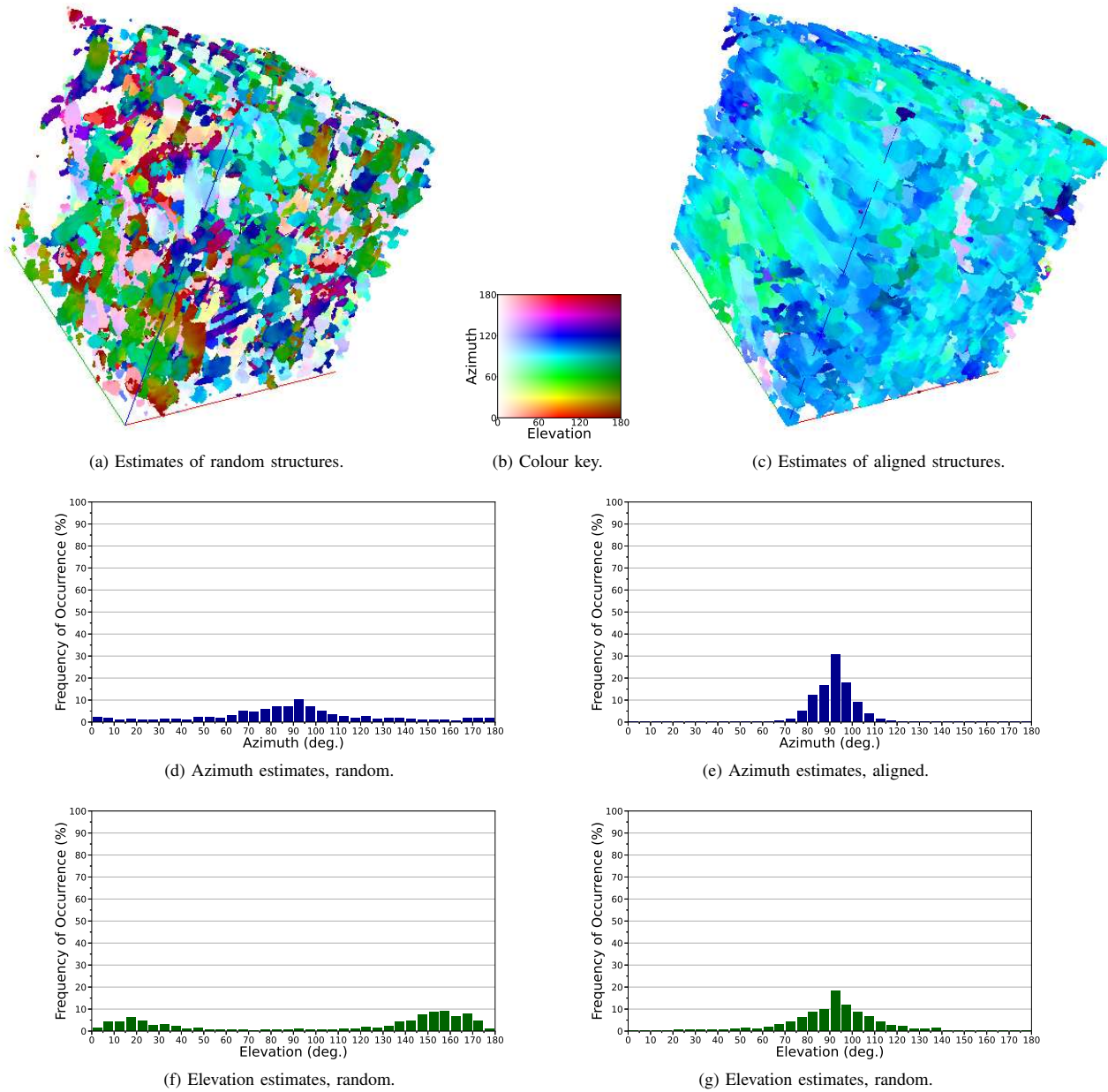(f) Elevation estimates, random.

(g) Elevation estimates, random.

Fig. 7. Results for real fibrous scaffold data from [10]. (a) The estimated orientations for the random structure dataset. (b) The colour key for elevation and azimuth combinations. (c) The estimated orientations for the aligned structure dataset. (d) and (f) the distributions of the estimated azimuth and elevation angles, respectively, for the random structures. (e) and (g) The distributions of the estimated azimuth and elevation angles, respectively, for the aligned structures.

random vectors," in *IEEE International Conference on Acoustics, Speech and Signal Processing*, 2008, pp. 3909–3912.

[13] T. Adali, P. J. Schreier, and L. L. Scharf, "Complex-valued signal processing: The proper way to deal with impropriety," *IEEE Transactions on Signal Processing*, vol. 59, no. 11, pp. 5101–5125, 2011.

[14] B. Selby, "Girdle distributions on a sphere," *Biometrika*, vol. 51, no. 3/4, p. 381, dec 1964.

[15] N. Fisher, T. Lewis, and B. Embleton, *Statistical Analysis of Spherical Data*. Cambridge University Press, 1987.

[16] K. Mardia and P. Jupp, *Directional Statistics*, ser. Wiley Series in Probability and Statistics. Wiley, 2009.

[17] B. Chaudhuri, P. Kundu, and N. Sarkar, "Detection and gradation of

oriented texture," *Pattern Recognition Letters*, vol. 14, no. 2, pp. 147–153, 1993.

[18] W. J. Karlon, P.-P. Hsu, S. Li, S. Chien, A. D. McCulloch, and J. H. Omens, "Measurement of orientation and distribution of cellular alignment and cytoskeletal organization," *Annals of Biomedical Engineering*, vol. 27, no. 6, pp. 712–720, 1999.